Chemical Engineering Journal 372 (2019) 1253–1264

Contents lists available at ScienceDirect

Chemical Engineering Journal

journal homepage: www.elsevier.com/locate/cej

How process parameters and packing materials tune chemical equilibrium and kinetics in plasma-based CO_2 conversion

Y. Uytdenhouwen[a,b,*], K.M. Bal[a], I. Michielsen[a,b], E.C. Neyts[a], V. Meynen[b], P. Cool[b], A. Bogaerts[a]

[a] Research Group PLASMANT, Department of Chemistry, University of Antwerp, Universiteitsplein 1, Wilrijk B-2610, Belgium
[b] Laboratory of Adsorption and Catalysis, Department of Chemistry, University of Antwerp, Universiteitsplein 1, Wilrijk B-2610, Belgium

HIGHLIGHTS

- Plasma-based CO_2 splitting is characterized in terms of equilibrium and kinetics.
- A shifted partial chemical equilibrium is established under plasma conditions.
- Equilibrium and kinetics are correlated and dependent on the process conditions.
- Addition of packing materials breaks the correlation of equilibrium and kinetics.
- Different materials tune the equilibrium and kinetics in their specific way.

ARTICLE INFO

Keywords:
Plasma
Dielectric barrier discharge
CO_2 dissociation
Chemical equilibrium
Chemical kinetics
Partial chemical equilibrium

ABSTRACT

Plasma (catalysis) reactors are increasingly being used for gas-based chemical conversions, providing an alternative method of energy delivery to the molecules. In this work we explore whether classical concepts such as equilibrium constants, (overall) rate coefficients, and catalysis exist under plasma conditions. We specifically investigate the existence of a so-called partial chemical equilibrium (PCE), and how process parameters and packing properties influence this equilibrium, as well as the overall apparent rate coefficient, for CO_2 splitting in a DBD plasma reactor. The results show that a PCE can be reached, and that the position of the equilibrium, in combination with the rate coefficient, greatly depends on the reactor parameters and operating conditions (i.e., power, pressure, and gap size). A higher power, higher pressure, or smaller gap size enhance both the equilibrium constant and the rate coefficient, although they cannot be independently tuned. Inserting a packing material (non-porous SiO_2 and ZrO_2 spheres) in the reactor reveals interesting gap/material effects, where the type of material dictates the position of the equilibrium and the rate (inhibition) independently. As a result, no apparent synergistic effect or plasma-catalytic behaviour was observed for the non-porous packing materials studied in this reaction. Within the investigated parameters, equilibrium conversions were obtained between 23 and 71%, while the rate coefficient varied between 0.027 s^{-1} and 0.17 s^{-1}. This method of analysis can provide a more fundamental insight in the overall reaction kinetics of (catalytic) plasma-based gas conversion, in order to be able to distinguish plasma effects from true catalytic enhancement.

Abbreviations: VOC, volatile organic compounds; NO_x, nitrogen oxide species; DRM, dry reforming of methane; ΔH^0_{298K}, standard reaction enthalpy; ΔG^0, Gibbs free energy of formation; DBD, dielectric barrier discharge; YSZ, Yttria-stabilized zirconia; SI, supporting information; PC, personal computer; P, power; n, number of consecutive periods; T, period; U, voltage; I, current; t, time; GHSV, gas hourly space velocity; GC, gas chromatograph; TCD, thermal conductivity detector; X, actual corrected conversion; X_{GC}, conversion according to uncorrected GC data; $\dot{y}$, molar flow rate of component y; S_n, sample standard deviation; $T(p, n_s)$, student's t-distribution for sample size n_s and probability p set at 95%; PCE, partial chemical equilibrium; C_a, concentration of species A; θ, derivative; z, length of the reactor; x, mole fraction; x_e, equilibrium mole fraction; x_i, initial mole fraction; k, rate coefficient; K, equilibrium constant; p, partial pressure; X_e, equilibrium conversion; t_e, time to equilibrium; SEI, specific energy input; E/N, reduced electric field; U_{RMS}, effective voltage; $x_{e,T}$, thermal equilibrium fraction; K_T, thermal equilibrium constant

* Corresponding author at: Universiteitsplein 1, B2.28, Wilrijk B-2610, Belgium.
E-mail address: yannick.uytdenhouwen@uantwerpen.be (Y. Uytdenhouwen).

https://doi.org/10.1016/j.cej.2019.05.008
Received 22 November 2018; Received in revised form 26 April 2019; Accepted 3 May 2019
Available online 04 May 2019

1. Introduction

Plasmas are increasingly being used for gas conversion in both research and industrial applications [1–5]. This includes (i) decomposition reactions, such as the destruction of large hydrocarbons, volatile organic compounds (VOCs), and smaller molecules like NOx [1,2]; as well as (ii) synthesis reactions, such as ozone production [3,4], dry reforming of methane (DRM) [5,6], and nitrogen fixation [7]. Plasmas offer a collision-rich environment, due to the presence of energetic electrons, which attack the stable molecules, to accommodate the otherwise high energy demand of highly endothermic reactions, such as CO_2 dissociation (ΔH^0_{298K} = 283 kJ/mol) and DRM (ΔH^0_{298K} = 247 kJ/mol), with an added high thermodynamic stability (strongly negative Gibbs free energy of formation, ΔG^0) of the reactants.

While traditional chemical reactors usually require harsh conditions, i.e., up to a few thousand Kelvin and/or hundred bars, to achieve sufficient conversion [5], generally in combination with a catalyst to enhance the kinetics, plasmas can offer similar conversions yet at much milder conditions. A dielectric barrier discharge (DBD) reactor in particular can operate at atmospheric, and slightly elevated pressure (up to several bar), and near room temperature, while the electron temperature can reach a value up to 10 eV (or ~110,000 K) [8], resulting in a non-thermal equilibrium environment. Indeed, various research groups have reported conversions up to 55% in the case of CO_2 dissociation [5,9–14] and up to 40% for DRM [15–19] in DBD reactors at ambient conditions, while traditional thermodynamics require a temperature of around 3100 K at 1 atm to achieve a conversion of 55% for CO_2 dissociation, and a temperature of 800 K to achieve 40% conversion for DRM [5]. Since the overall temperature of the gas remains below 500 K for powers up to 100 W in a DBD reactor at 1 atm [10,14], the thermal thermodynamic equilibrium is still pointing strongly towards the highly stable reactant molecules (CO_2), which would give rise to no appreciable conversion in a thermal process. This suggests that plasma chemistry is governed by a partial chemical equilibrium different from the thermal thermodynamic equilibrium at the same pressure and temperature, an apparent equilibrium that depends on the plasma operating conditions and reactor parameters [20–22]. Our previous work has indicated this behaviour for a micro DBD reactor, with a gap size of 455 μm and plasma power of 30 W [14], for the dissociation of CO_2 into CO and O_2, where the conversion increased with increasing residence time up to 30 s and then reached a plateau value of around 50–55%.

The introduction of (catalytic) packing materials into plasma reactors is an obvious step to further enhance conversions and to selectively steer multi-product reactions. Numerous papers showed promising results with increased conversions, leading to terms such as “synergistic effect” and “plasma catalysis” making the scene [5,7,23-26]. Unlike thermal catalysis, where the catalyst only modifies the kinetic parameters of the process, the combined application of a catalyst with a non-thermal-equilibrium plasma has the potential to simultaneously affect the reaction rate, as well as the position of the equilibrium. This is because the (catalytic) packing material can influence the plasma behaviour (e.g. electric field enhancement, altering the electron density and temperature, and changing the discharge type), and vice versa, the plasma can modify the material properties (e.g. reactions with the surface, causing activation, modifications, or alternative pathways), as discussed by Neyts and Bogaerts [27]. In addition, packing materials introduce macro porosity in between the spheres, as well as meso porosity inside catalyst pores, in which plasma can be generated, depending on the pore size, material properties, and gas [28–30]. Nevertheless, since most experiments have only probed a limited range of flow rates and residence times, little is known about the specific effect of packing materials on equilibrium and kinetics, as it is difficult to separate these effects in common experimental observations.

The observation of equilibrium-like behaviour in plasma-based gas conversion raises the question how far, exactly, this analogy with thermal reactions can be taken. That is, to what extent can concepts such as equilibrium concentrations and constants, (overall) rate coefficients, and catalysis be applied to chemical processes in the inherently non-thermal-equilibrium environment of a plasma? And how do the plasma and process parameters, as well as (catalytic) packing materials, affect these concepts? Being able to assign common equilibrium and kinetic concepts to plasma-based reactions would make it possible to directly compare the intrinsic performance of different plasma reactors (as well as with other technologies, e.g., thermal approaches) on a fundamental level, using the same measuring stick.

In this work, we explicitly investigated the apparent chemical equilibrium-like behaviour (or so-called partial chemical equilibrium), as well as the kinetic parameters, of the CO_2 dissociation reaction in a DBD plasma reactor, by performing conversion experiments for a broad range of residence times. Using this methodology, we investigate how the global chemical equilibrium and conversion rate can be tuned through modification of the plasma, reactor parameters, and operating conditions (*in casu* the plasma power, gas pressure, gap size), and introduction of packing materials.

2. Methods and theory

2.1. Experimental set-up

A cylindrical DBD (micro gap) reactor was used, as shown in Fig. 1, with a stainless-steel rod with different diameters of 16.50, 14.95, and 8.00 mm as the central (and grounded) electrode. An alumina dielectric tube, with a precision honed inner diameter of 17.41 mm and a wall thickness of 2.5 mm, was placed over the rod to shape the reaction volume and create different discharge gaps of 455, 1230, and 4705 μm, respectively. A stainless-steel mesh with a length of 100 mm was wrapped around the dielectric as the high voltage electrode. The resulting empty reaction volumes are 2.424×10^3, 6.252×10^3, and 18.780×10^3 mm^3. The 455 and 4705 μm reactors were also filled with a non-porous spherical packing material made of SiO_2 and ZrO_2 (YSZ, yttria-stabilized zirconia) (both Sigmund Lindner), with a size range of 100–200 μm and 1600–1800 μm in the respective discharge gaps, resulting in similar sphere-to-gap ratios of 0.33 and 0.36.

A high voltage amplifier (TREK, Model 20/20C-HS, x2000 voltage amplification), driven by a PC controlled function generator (Tektronix, AFG 2021) fixed at 3 kHz, was used to operate the high voltage electrode. Adjusted amplitudes were used to load the reactor with an effective plasma power between 5 and 45 W. The power was continuously recorded by a digital oscilloscope (Picotech, Picoscope 6402D) to adjust the amplitude to the desired power. A high voltage probe (Tektronix, P6015A) was used to monitor the applied voltage, in combination with a current transformer (Pearson, Model 4100) to monitor the current profile, in order to calculate the power during a number (n) of consecutive periods (T):

$$P = \frac{1}{nT}\int_0^{nT} U(t)I(t)dt \quad (1)$$

The gas feed consisted of either a pure CO_2 stream or a 2/3 CO and 1/3 O_2 mixture, in order to study both the forward and back reaction of CO_2 conversion, and to gain more information on the equilibrium-like behaviour. Gas flow rates were set and controlled by mass flow controllers (Bronkhorst EL-FLOW Select series) to provide the required flow rates between 1 and 400 mL/min, that based on the reactor volume, results in specific residence times desired in the experiments. A correction needs to be applied in the case of a packed reactor, since the added packing material reduces the effective reaction volume. Calculations of spheres filling the coaxial reactor of this work in MATLAB revealed the actual packing efficiency to be 49.51 ± 0.02% in the case of 100–200 μm spheres in the 455 μm gap, and 48.27 ± 0.07% in the case of 1.6–1.8 mm spheres in the 4705 μm gap. These values differ considerably from the maximum spherical packing

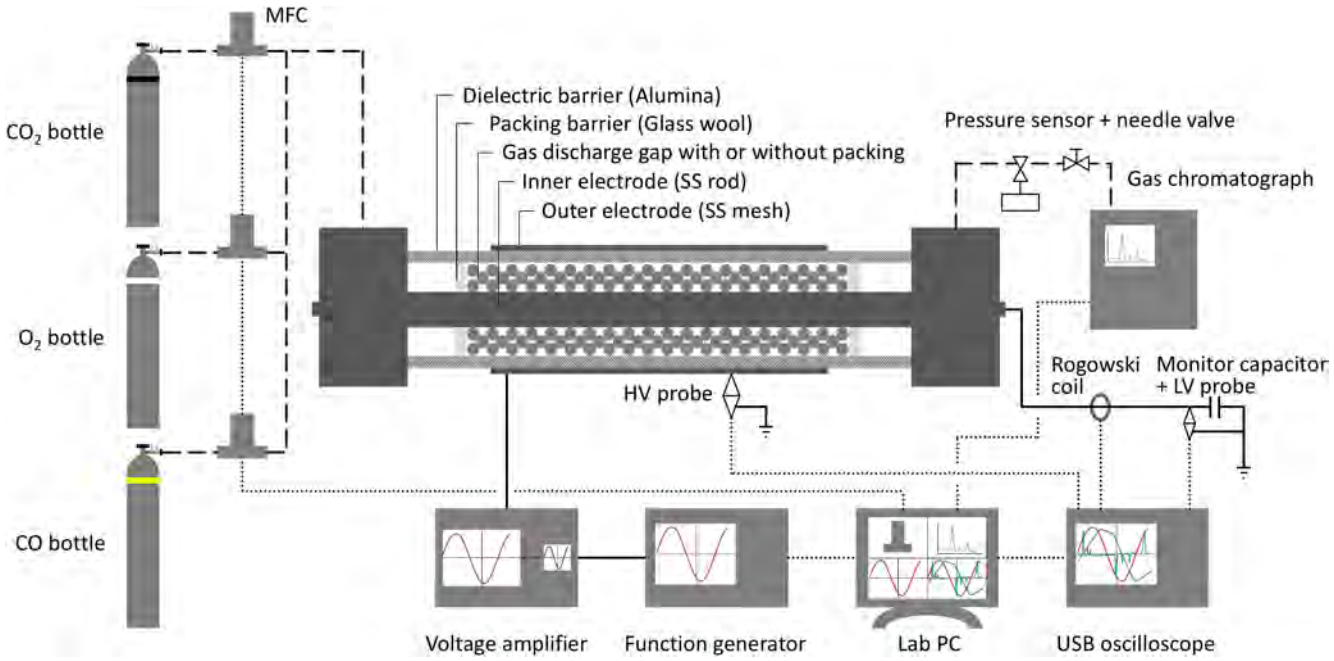

Fig. 1. DBD (micro) plasma reactor used in this work with analytical equipment.

efficiency of 74.048% in case of a close packing, due to sphere-wall interactions and a more realistic filling behaviour in the calculations in case of finite reactor volumes, such as in our DBD reactor. These adjusted packing efficiencies were used to determine the flow rates for corresponding residence time. A more detailed explanation of the calculation can be found in the Supplementary information. Note that the results can easily be converted to gas hourly space velocity (GHSV) with the values above if desired and will match the reciprocal of the residence time.

Gas analysis was performed by a gas chromatograph (Compact GC, Interscience) with pressure-less sampling. This GC features a thermal conductivity detector (TCD) channel, able to measure the CO and O_2 composition as one peak and the CO_2 composition separated by an Rt-Q-Bond column. No significant amounts of ozone and carbon deposition were detected. The CO_2 or total CO + O_2 conversion derived from the GC data was defined as:

$$X_{GC,y} = \frac{\dot{y}_{\text{in}} - \dot{y}_{out}}{\dot{y}_{in}} \tag{2}$$

With $\dot{y}$ the molar flow rate of component y, being either CO_2 or CO + O_2. This conversion value must be corrected for a pressure-less sampling set-up, due to gas volume expansion in the case of CO_2 dissociation. It has been previously shown by Pinhão et al. [18] and Snoeckx et al. [31] that the actual CO_2 conversion (X_{CO_2}), in a pure CO_2 system, can be calculated by:

$$X_{GC,CO_2} = 1 - \left(\frac{1 - X_{CO_2}}{1 + \frac{X_{CO_2}}{2}} \right) \Leftrightarrow X_{CO_2} = \frac{2\, X_{GC,CO_2}}{3 - X_{GC,CO_2}} \tag{3}$$

Vice versa, in the case of the back reaction, i.e., CO oxidation, the conversion value calculated in Eq. (2) must be corrected for gas volume reduction. Based on the same method as for Eq. (3), we formulated a new expression to calculate the actual CO conversion by:

$$X_{GC,CO+O_2} = 1 - \left(\frac{1 - X_{CO+O_2}}{1 - \frac{X_{CO+O_2}}{3}} \right) \Leftrightarrow X_{CO+O_2} = \frac{3\, X_{GC,CO+O_2}}{2 + X_{GC,CO+O_2}} \tag{4}$$

A needle valve and pressure sensor (Type TK, Gefran) placed between the reactor and the GC were used to regulate an extra pressure drop to the system at the beginning of the experiment when a higher reactor pressure than atmospheric pressure was desired. Otherwise, it was kept in its fully open position, resulting in no significant pressure drop.

2.2. Experimental method

The reactor was operated for a minimum amount of time of 40 min, to let it reach a thermal steady-state behaviour. Extended operating times up to 120 min were used for flow rates lower than 10 mL/min, to ensure steady-state behaviour in the reactor and following tubing, for consistent gas composition analysis. The applied voltage was periodically adjusted on the function generator to obtain and maintain the desired constant plasma powers between 5 and 45 W. Four GC and oscilloscope measurements were recorded as soon as steady-state behaviour was reached.

Every condition was tested in threefold for statistical review, resulting in twelve data points per condition. The error bars were defined as:

$$error = \pm S_n \frac{T(p,\, n_s)}{\sqrt{n_s}} \tag{5}$$

With S_n the sample standard deviation of the measurements, n_s the sample size (12), and T the two-tailed inverse of the Student's t-distribution for sample size n_s and probability p set at 95%.

2.3. Partial chemical equilibrium

The plasma in the DBD reactor is not in thermal equilibrium, which means that standard equilibrium thermodynamics is not applicable. However, as pointed out by Vepřek and co-workers, a kind of chemical equilibrium can still be reached in such a case [20–22]. This *partial chemical equilibrium* (PCE) state differs from a general chemical kinetic state because it corresponds to a unique gas composition for a given set of process conditions. A kinetic steady state can be achieved at any point in the reactor, provided that the local concentration C_A of any species A remains constant in time, i.e., $\partial C_A/\partial t = 0$. However, as long as the total consumption and production rates of A are not equal, a

concentration gradient along the length of the reactor z will exist, so that $\partial C_A/\partial z \neq 0$. In a PCE state, one will also have $\partial C_A/\partial z = 0$, because the total chemical flux (combined consumption and production rate) is zero. As such, a PCE state fulfils the requirement of chemical equilibrium (consumption and production reaction rates are equal). Furthermore, the PCE can be reached from the reagent and the product side of the equilibrium, unlike any of the other steady states encountered in the reactor. The particular equilibrium composition in the reactor does not reflect any thermal thermodynamic equilibrium, but is dictated by the plasma conditions (energy added as electricity). This plasma-induced equilibrium shift explains why thermal thermodynamically forbidden conversions can still take place inside a plasma.

The PCE state can be used to uniquely characterize a plasma-based conversion process, because it directly depends on the plasma conditions. Introduction of the PCE concept to plasma conversion processes also offers a simple way to extract both the maximum conversion achievable in the plasma (which can be obtained from the PCE gas composition), and the overall conversion rate (i.e., the rate of evolution towards PCE) for an arbitrary reaction. As such, “thermodynamic” and “kinetic” effects can be separated or, more correctly, the characteristic shift in chemical equilibrium due to the non-equilibrium plasma can be distinguished from the increased conversion rate caused by reactive plasma chemistry or (catalytic) packing materials. This study allows to gain deeper insight, in stark contrast with many previous studies of plasma conversion (including our own), where different process conditions were typically compared at fixed residence time. Indeed, in the latter case, it was not possible to unambiguously relate changes in conversion to either changes in rate (or catalytic effects) on one hand, or shifts in the intrinsic conversions on the other hand.

Assuming that both the production and consumption of any species in the plasma reactor can be described as a single (lumped, effective) first order process, its mole fraction can then be correlated with the residence time, t, through a general expression:

$$x_y(t) = x_{e,y} - (x_{e,y} - x_{i,y})e^{-k_y t} \quad (6)$$

with x_y the mole fraction of component y, $x_{e,y}$ the mole fraction at PCE, $x_{i,y}$ the initial mole fraction at $t = 0$, and k_y the overall apparent reaction rate coefficient. Because the PCE should be reachable from either side of the reaction, $2CO_2 \leftrightarrow 2CO + O_2$, it is possible to fit either the CO_2 conversion (forward reaction, starting from $x_{i,CO_2} = 1$), or the O_2 conversion (back reaction, starting from $x_{i,O_2} = 1/3$, but an analogous expression could also use the CO conversion). Although up to a thousand reactions [9,32–34] could be considered for the CO_2 plasma chemistry, drastic assumptions were made to simplify the fitting procedure, and no explicit mechanistic information is used to construct the expression—the only purpose of the analysis is to extract a small number of global parameters for each condition, allowing to more directly compare the different conditions. Therefore, the rate coefficient is assumed to be the overall apparent reaction rate coefficient for the forward or back reaction. The full derivation of the fit equation can be found in the Supplementary information.

The experimental data (consisting of up to 132 data points per parameter and reaction) were first converted into mole fractions as stated above, subsequently imported into MATLAB, where a fit was calculated according to Eq. (6), and finally converted back into conversions. From the resulting fit, the equilibrium conversions and apparent rate coefficients of the forward and back reactions can thus be directly obtained, and hence also the equilibrium constant, from:

$$K = \frac{p_{CO}^2 p_{O_2}}{p_{CO_2}^2} \quad (7)$$

With p the partial pressure calculated based on the final CO_2 conversion for p_{CO2} and on the total CO + O_2 conversion for p_{CO} and p_{O2}. The results of the data fits are always plotted below with their respective 95% confidence interval. Finally, the time needed to reach the equilibrium conversion was calculated based on the data fit. This was arbitrarily defined when the mole fraction of CO_2 (for the forward reaction) and O_2 (for the back reaction) reaches a value of 1.02 times the equilibrium mole fraction calculated by the fit. Equivalently, 98% of the equilibrium conversion can be used as the threshold value.

3. Results and discussion

Three series of experiments were performed in order to investigate the research questions postulated in the introduction. First, the existence of an equilibrium-like behaviour was tested by performing both forward and back reaction experiments of CO_2 dissociation, with a residence time up to 75 s (Section 3.1). The equilibrium and the associated kinetics were further examined by changing various reactor parameters and operating conditions (Section 3.2), and finally by investigating the effect of (catalytic) packing materials (Section 3.3). Various conditions were tested and compared with the reference measurements at 30 W, 455 µm gap size, 1 bar, and without packing material.

3.1. CO_2 splitting can reach a partial chemical equilibrium

CO_2 dissociation and CO oxidation experiments were performed, starting from either pure CO_2 or a 2/3 CO + 1/3 O_2 mixture, respectively, in a 455 µm gap size DBD reactor. Three different powers were used, i.e. 15, 30, and 45 W, in an extended residence time range up to 75 s. The results of these experiments are shown in Fig. 2. The total CO + O_2 conversion is plotted on a reverse order y-axis (100 → 0% conversion) to visualize any partial chemical equilibrium behaviour, i.e. reaching the same chemical equilibrium composition as the forward reaction (CO_2 conversion). Since only traces of unwanted side products, such as carbon and ozone, were detected in this elementary reaction by lack of carbon deposition and test tubes respectively, we can assume that the composition, and conversion, at chemical equilibrium is related as:

$$X_{e,CO_2} = 1 - X_{e,CO+O_2} \quad (8)$$

The results for the plasma dissociation of CO_2 into CO and O_2, displayed in Fig. 2, show that for each applied power a plateau is reached between 50 and 60% conversion after a certain residence time, as was also seen in our previous work [14]. In this overall reaction, it can be assumed, based on CO_2 plasma chemistry simulations in a DBD by Aerts et al. [9,32], that the CO_2 conversion is mainly attributed to electron impact dissociation of CO_2 into CO and O, followed by three-body recombination of 2 O atoms (and a third heavy particle) into O_2. As the residence time increases and more CO is created, the back reaction (i.e., CO oxidation) will become more significant, and CO and O_2 start to be converted back into CO_2. This is initiated by electron impact dissociation of O_2 into 2 O atoms, followed by the three-body recombination of CO and O (with a third heavy particle) into CO_2. When the gas mixture spends more time in the plasma reactor, the overall rate of CO_2 dissociation decreases, while the overall rate of CO oxidation increases, until they match and an equilibrium is reached.

In practice, this process is a bit more intricate, due to the filamentary behaviour of a DBD that exhibits short plasma pulses in the form of micro discharges, which typically last for a few hundred nanoseconds [4]. The latter gives rise to a sequential intermittent behaviour, where first small fractions of gas, both reagent(s) and product(s), are continuously turned into plasma channels (typically 100 µm radius [4]), in which the forward and back reactions can take place. This excited state of the gas fractions is then followed by a “cool-down” in between two micro discharges. In an ideal plug-flow-like DBD reactor with the width of one plasma channel, this would mean a stepwise conversion of reactants as a function of time or distance in the reactor (cf. Fig. 7 in [32]) until the rates of forward and back reaction are equal and an equilibrium conversion is reached. However, in a real DBD reactor, the

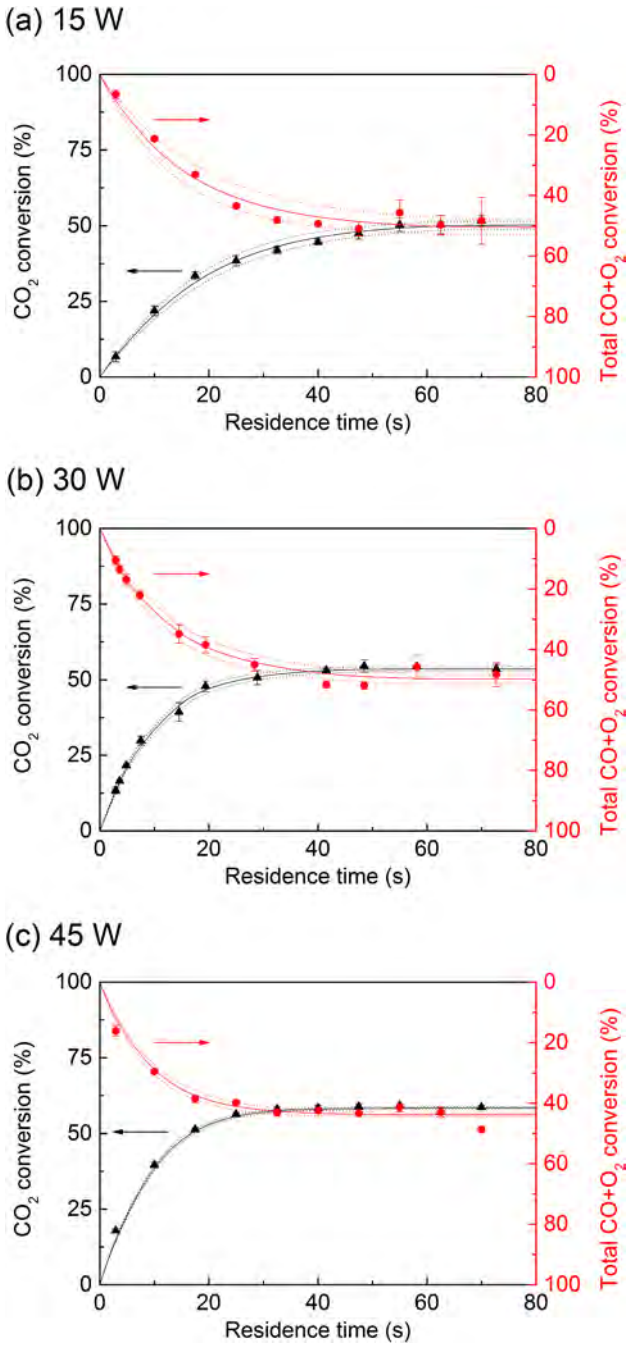

Fig. 2. CO_2 conversion (black triangles) and total CO + O_2 conversion (red circles) in a 455 µm gap size, plotted as a function of residence time for (a) 15 W, (b) 30 W, and (c) 45 W. An apparent first-order reversible reaction fit for both forward and back reaction is applied (solid lines) with its 95% confidence interval (dotted lines).

limited amount of micro discharges per period are spread out over the whole reaction volume. This filamentary behaviour, giving rise to a limited number of small reaction channels during short frames, leads to the possibility of gas fractions taking shortcuts through the reactor, where molecules might never be turned into the plasma phase if gas mixing by radial and axial diffusion of gas molecules is limited, or the residence time is too short. The reactor does eventually exhibit an equilibrium value when enough time is given, where the forward reaction rate, back reaction rate and the non-ideal ("real") behaviour converge. In other plasma reactor types, similar intermittent behaviour is apparent, e.g., by subsequent arc discharges (gliding arc reactor [35]) or only once by one homogeneous discharge zone (e.g., glow or microwave discharge reactor [36]).

Similar to the CO_2 splitting process, CO oxidation reaches a plateau after a certain residence time, as evidenced by the total CO + O_2 conversion depicted in Fig. 2. Moreover, the apparent equilibrium conversion X_{CO} of the CO oxidation reaction is equal to the value of $1 - X_{CO_2}$ as obtained from the CO_2 splitting reaction. Both processes thus lead to the same gas composition at each tested plasma power. Therefore, we can conclude that plasma-based CO_2 splitting can, in fact, be characterized by its PCE state, which is very different from the thermodynamic equilibrium under thermal conditions, and explains the high CO_2 conversion attainable in a DBD plasma near room temperature.

It should be noted that the specific energy input per mole of CO_2 (defined as the ratio of plasma power over volumetric flow rate) increases drastically with increasing residence time (2.9–70 s) from 36 to 900 kJ/L in the case of 30 W. Therefore, when judging these results based on the energy efficiency, longer residence times have a very negative performance, in spite of their higher conversion. This was discussed in more detail in our previous work for CO_2 dissociation at 30 W plasma power [14], and will therefore not be further discussed here.

3.2. Tuning equilibrium and kinetics in plasma-based gas conversion

In this section, we investigate how three of the most important process parameters, i.e. power, pressure, and gap size, influence the equilibrium and kinetics of the CO_2 dissociation reaction in the DBD (micro) plasma reactor. From this section on, we will only focus on the forward reaction, since Section 3.1 already proved that the back reaction behaves towards the same equilibrium, and the eventual reaction of interest is the dissociation reaction.

3.2.1. Influence of power

Section 3.1 showed that plasma-based equilibria can be reached in a plasma reactor, and hinted that the time to reach equilibrium, as well as the equilibrium value, depends on the plasma power. The CO_2 conversion data for the three different powers, i.e. 15, 30, and 45 W, are grouped in Fig. 3(a), to further investigate the differences.

From this figure, we can conclude that the deposited plasma power positively influences the equilibrium conversion, bringing it from around 50% at 15 W to almost 60% at 45 W. Simultaneously, the overall reaction rate also increased, as evidenced by the steeper gradient of the curves with respect to the residence time, which means that partial chemical equilibrium is reached faster. This is confirmed by the apparent first-order reversible reaction fit (Eq. (6)), plotted as the solid lines with their respective 95% confidence interval, and the retrieved data shown in Table 1. The derived fit equation is in very good agreement with the experimental data, validating the simplified model. The fit shows that indeed the equilibrium conversion for CO_2 dissociation increases with power, from 51% at 15 W, to 58.4% at 45 W (see Table 1). The reaction equilibrium constant K, calculated with Eq. (7), is therefore found to be 0.22 for 15 W, 0.28 for 30 W, and 0.45 for 45 W (see Table 1). The calculated apparent reaction rate coefficients confirm the observations made above. The overall rate coefficient for CO_2 dissociation doubles from 0.064 to 0.139 s^{-1} when increasing the power from 15 to 45 W, with the largest increase from 15 to 30 W. As a result, we also see a drop in the time needed to reach the equilibrium conversion, since a higher power results in higher rate coefficients without a massive increase of the equilibrium conversion, ensuring a shorter time towards equilibrium. The time to reach equilibrium is reduced by a factor 2 upon increasing power from 15 to 45 W, i.e. from 68.1 s at 15 W to 33.6 s at 45 W. In conclusion, the plasma power can tune both the position of the equilibrium and the overall reaction rate, although not independent of each other.

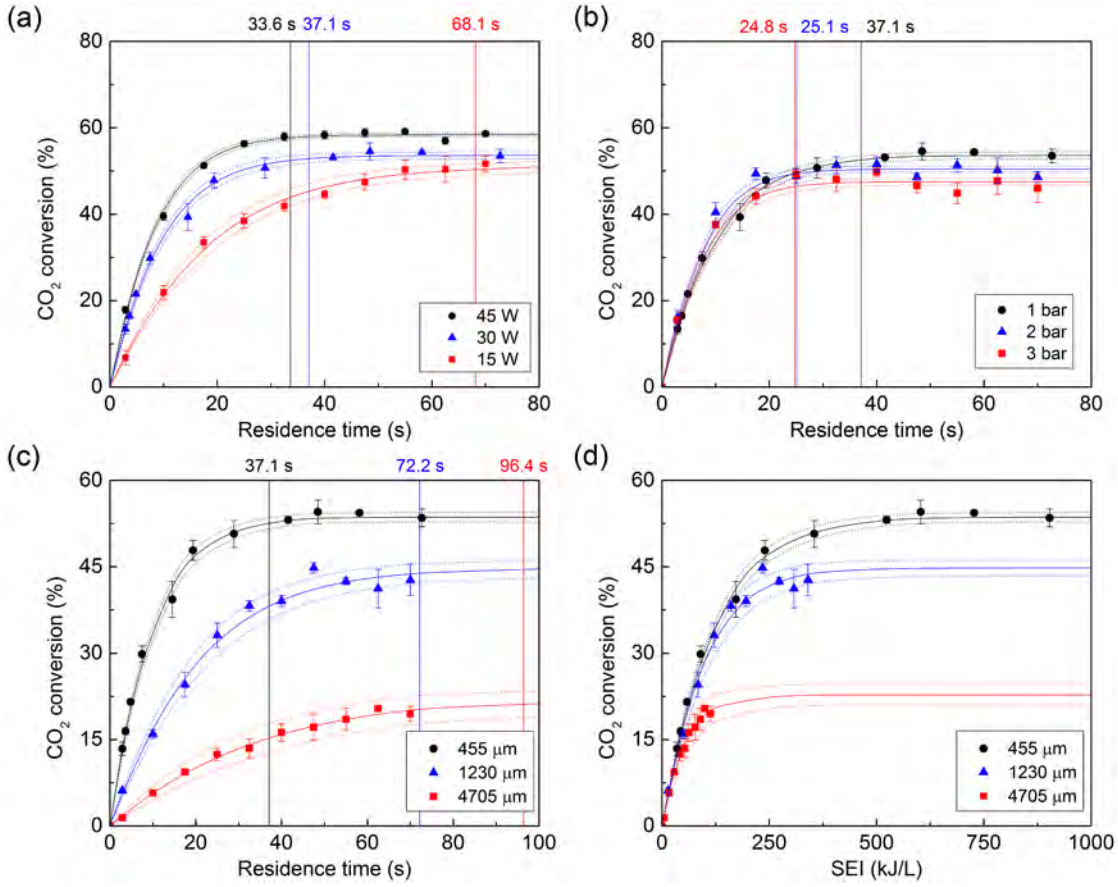

Fig. 3. CO_2 conversion, plotted as a function of residence time, (a) in a 445 µm gap size at 1 bar, for 15 W, 30 W, and 45 W, (b) in a 445 µm gap size at 30 W, for 1 bar, 2 bar, and 3 bar, (c) at 30 W and 1 bar, for a gap size of 455 µm, 705 µm, and 4705 µm. In (d), the same data as in (c) are plotted, rescaled as a function of SEI. An apparent first-order reversible reaction fit is applied for all graphs (solid lines) with its 95% confidence interval (dotted lines). The time point at which the fit in (a), (b), and (c) reaches 98% of the end conversion of CO_2 dissociation is indicated for each case by the vertical line.

Table 1
Fitted kinetic and equilibrium data for the CO_2 splitting reaction, at a plasma power of 15, 30, and 45 W, in a 455 µm gap size at 1 bar. The retrieved data are the equilibrium constant K, calculated from the Xe values, as well as the apparent reaction rate coefficient k, equilibrium conversion Xe, and time to equilibrium conversion t_e.

Plasma power (W)	15	30[a]	45
K	0.22 ± 0.02	0.28 ± 0.02	0.45 ± 0.02
k (s^{-1})	0.064 ± 0.004	0.120 ± 0.005	0.139 ± 0.004
X_e (%)	51 ± 1	53.6 ± 0.8	58.4 ± 0.4
t_e (s)	68.1	37.1	33.6

[a] Denoted as standard reference A throughout all measurements (see Section 3.3 below).

Table 2
Fitted kinetic and equilibrium data for the CO_2 splitting reaction, at a reactor pressure of 1, 2, and 3 bar, in a 455 µm gap size at 30 W. The retrieved data are the equilibrium constant K, calculated from the Xe values, as well as the apparent reaction rate coefficient k, equilibrium conversion Xe, and time to equilibrium conversion t_e.

Pressure (bar)	1[a]	2	3
K	0.28 ± 0.02	0.42 ± 0.03	0.47 ± 0.04
k (s^{-1})	0.120 ± 0.005	0.17 ± 0.01	0.17 ± 0.01
X_e (%)	53.6 ± 0.8	50.5 ± 0.7	47.5 ± 0.8
t_e (s)	37.1	25.1	24.8

[a] Denoted as standard reference A throughout all measurements (see Section 3.3 below).

3.2.2. *Influence of pressure*

The reactor pressure in a DBD is typically kept constant at atmospheric pressure. Indeed, increasing the pressure has a negative influence on the gas breakdown and subsequent discharge sustainment through Paschen's law [37]. It is nonetheless a valuable parameter to investigate, due to the widespread use of high-pressure processes in industrial settings. Thus, we performed experiments at a reactor pressure of 1, 2, and 3 bar, by adjusting a needle valve to add an extra pressure drop in the system.

The results plotted in Fig. 3(b) do not reveal significant differences at first glance, except for a slight change in equilibrium conversion. Applying the simplified model fit to the data, with the retrieved data displayed in Table 2, reveals the influence of the pressure in more detail. First of all, a higher pressure results in a drop in equilibrium conversion from 53.6% at 1 bar, to 47.5% at 3 bar. This is expected based on Le Chatelier's law, dictating that higher pressures move the equilibrium to the side with the least amount of molecules, thus promoting the back reaction more than the forward reaction. However, due to the stoichiometry of the reaction, we would expect the conversion to drop much more. In traditional thermodynamics, the pressure-based equilibrium constant K, as used here, should remain constant as the pressure increases, dictating a theoretical drop in equilibrium conversion from 53.6% at 1 bar, over 46.4% at 2 bar, to 42.3% at 3 bar. This suggests that the higher pressure has some positive effect on the plasma characteristics to counteract the behaviour of the standard thermal chemical equilibrium. Of course, standard thermal equilibrium thermodynamics cannot be invoked, which might explain this discrepancy.

In addition to the relatively mild drop in equilibrium conversion

(see Table 2), a higher pressure enhances the reaction rate. The rate coefficient increases from 0.120 s^{-1} at 1 bar, to 0.17 s^{-1} at 2 bar and keeps that value upon increasing the pressure to 3 bar (see Table 2). The higher pressure yields more collisions between the plasma species, due to their higher densities, enhancing the rate coefficient, but it quickly reaches the limits of this reaction pathway. In theory, this higher pressure could enhance three-body reactions, but this is not consistent with the capped rate coefficient in this pressure region, indicating that rate-determining processes are primarily electronic.

The results show that increasing the pressure from 1 to 2 bar is more beneficial to enhance the rate coefficient than increasing the plasma power from 30 to 45 W (cf. Tables 1 and 2). As a result, the time to equilibrium is shortened from 37.1 s to around 25 s, when raising the pressure from 1 to 2 bar, at the same plasma power of 30 W. Hence, we can conclude that the relatively small pressure increase can also tune both the equilibrium properties and the reaction rate (at least when varying from 1 to 2 bar), although in a different way, i.e., a higher pressure yields a lower equilibrium constant, but a higher rate coefficient, while a higher power resulted in both a higher equilibrium constant and reaction rate coefficient (see previous section).

3.2.3. Influence of gap size

Finally, we investigated the effect of the discharge gap size. Our previous paper already touched on this subject by revealing that a longer residence time and smaller gap size resulted in an enhanced CO_2 conversion, due to a higher reduced electric field and specific energy input (SEI) [14]. However, in [14] we only considered two different residence times (i.e. 7.5 s and 28.9 s). Here, we study this effect in more detail, by extending over a larger residence time, for a gap size of 455, 1230, and 4705 μm.

Fig. 3(c), and the retrieved reaction parameters in Table 3, show the largest changes so far. A larger gap size drastically decreases the equilibrium conversion, from 53.6% at 455 μm to only 23% at 4705 μm. This is due to the lower SEI applied to reach the same residence time, and thus the lower reduced electric field, leading to fewer and less powerful discharges, as explained in our previous work [14]. We also plot the conversion as a function of SEI in Fig. 3(d), to illustrate the scale of different SEI values used in these experiments. These different SEI values are reached by applying different flow rates, as we apply a constant plasma power of 30 W. We can see that the conversions in the three gaps match each other very closely at low SEI values (i.e., high flow rates), which means that the overall efficiency of each reactor is similar, although the reaction volume is more efficiently used at smaller gap sizes. At higher SEI values, the limiting effect of the gaps comes into play and determines the maximum conversion that can be reached. The efficient use of the gap size is observed as well from the lower rate coefficients upon increasing the gap size (see Table 3). The rate coefficient decreases from 0.120 s^{-1} at 455 μm, taking 37.1 s to reach equilibrium conversion, to only 0.032 s^{-1} at 4705 μm, taking 96.4 s. A smaller gap size is therefore advised, since a larger gap is associated with a lower CO_2 dissociation rate and a lower maximum conversion.

Table 3
Fitted kinetic and equilibrium data for the CO_2 splitting reaction, at a gap size of 455, 1230, and 4705 μm, at 30 W and 1 bar. The retrieved data are the equilibrium constant K, calculated from the Xe values, as well as the apparent reaction rate coefficient k, equilibrium conversion Xe, and time to equilibrium conversion t_e.

Gap size (μm)	455 [a]	1230	4705 [b]
K	0.28 ± 0.02	0.12 ± 0.02	0.009 ± 0.002
k (s^{-1})	0.120 ± 0.005	0.057 ± 0.005	0.032 ± 0.005
X_e (%)	53.6 ± 0.8	45 ± 1	23 ± 2
t_e (s)	37.1	72.2	96.4

a, b: Denoted as standard reference A and B throughout all measurements (see Section 3.3 below).

3.3. Distinguishing catalytic effects from plasma chemistry

In traditional (thermal) catalysis, a catalyst can provide a surface chemical reaction with an alternative reaction pathway with a lower energy barrier, which enhances the overall reaction rate coefficient without altering the underlying thermodynamic equilibrium. Because (catalytic) packing materials can also change the plasma properties [27], we can expect that the introduction of a packing will have a much more complicated impact on a plasma-based conversion process. Indeed, even experiments with identical packing materials have shown very different trends when using different gap sizes [14]. We therefore performed here two sets of experiments, employing reactors with a gap size of 455 μm and 4705 μm, respectively, both packed with either non-porous SiO_2 or ZrO_2 spheres. By explicitly untangling the effects of kinetics and shifting chemical equilibrium, we hope to elucidate to what extent the influence of a packing material can be purely catalytic (only changing the kinetics), or if the plasma–packing interplay is more complex (and the equilibrium is also shifted).

3.3.1. Influence of packing material in a 455 μm discharge gap

The first set of experiments was performed in a 455 μm gap, with both SiO_2 and ZrO_2 spheres with a size range of 100–200 μm, and the results were compared to the reference empty reactor discussed in previous Section 3.2. In our previous work we found that, at a constant residence time of 7.5 s, SiO_2 can enhance the CO_2 conversion in comparison with an empty reactor, whereas small (100–200 μm) ZrO_2 spheres have no impact on the conversion [14]. We now expand these results to the whole residence time range, as shown in Fig. 4(a), with the retrieved reaction parameters in Table 4.

It is clear from Fig. 4(a) and Table 4 that the two packing materials exhibit an unexpected behaviour. SiO_2 enhances the equilibrium conversion from 53.6% to an impressive 71.1%, which is to our knowledge the highest reported CO_2 conversion in a DBD reactor so far, although it must be realized that this record value in conversion is accompanied by a low energy efficiency. Simultaneously, SiO_2 slightly lowers the overall reaction rate coefficient from 0.120 s^{-1} to 0.111 s^{-1}. ZrO_2, on the other hand, does not significantly enhance the equilibrium conversion, when taking the error bars into account, but it drastically lowers the rate coefficient from 0.120 s^{-1} to only 0.050 s^{-1}. These results show that introduction of these packing materials does not accelerate the kinetics in this reactor. Hence, this implies that it cannot be assumed that the packing merely leads to the creation of small voids that induces a reduced gap effect, since a smaller gap enhances the rate coefficient, as seen in Section 3.2.3. On the contrary, it suggests that the main reaction pathways—electron impact reactions in a DBD—are at least partially inhibited under the applied conditions here. This can have many causes, such as a lower electron density as a result of more surface losses [38], or perhaps due to a change in discharge type [39], and this seems even more pronounced for ZrO_2 than for SiO_2. Such an observation is indeed supported by fluid modelling studies of Van Laer and Bogaerts [40] who showed that packing materials with higher dielectric constants (such as ZrO_2) lead to a drastic decrease of the electron density in this type of reactor (with the same gap size) (cfr. Fig. 6 in their work), which in turn lowers the dissociation rate of CO_2 (cfr. Fig. 11 in their work). At the same time, however, the packing can increase the maximum conversion, as clearly demonstrated in Fig. 4(a) for SiO_2, which can be correlated by a slight elevation of the electron temperature (also predicted by the modelling of Van Laer and Bogaerts [40]), that allows putting more energy into the system and pushing the conversion equilibrium of this endothermic reaction further to the right.

Rescaling the results as a function of the SEI (i.e., the inverse of the flow rate, as we keep the power constant) reveals that at low SEI (high flow rate) the empty reactor is more efficient in converting CO_2 than the packed reactors, due to its higher rate coefficient, as seen in Fig. 4(b). At higher SEI (lower flow rate) the packed reactors start to

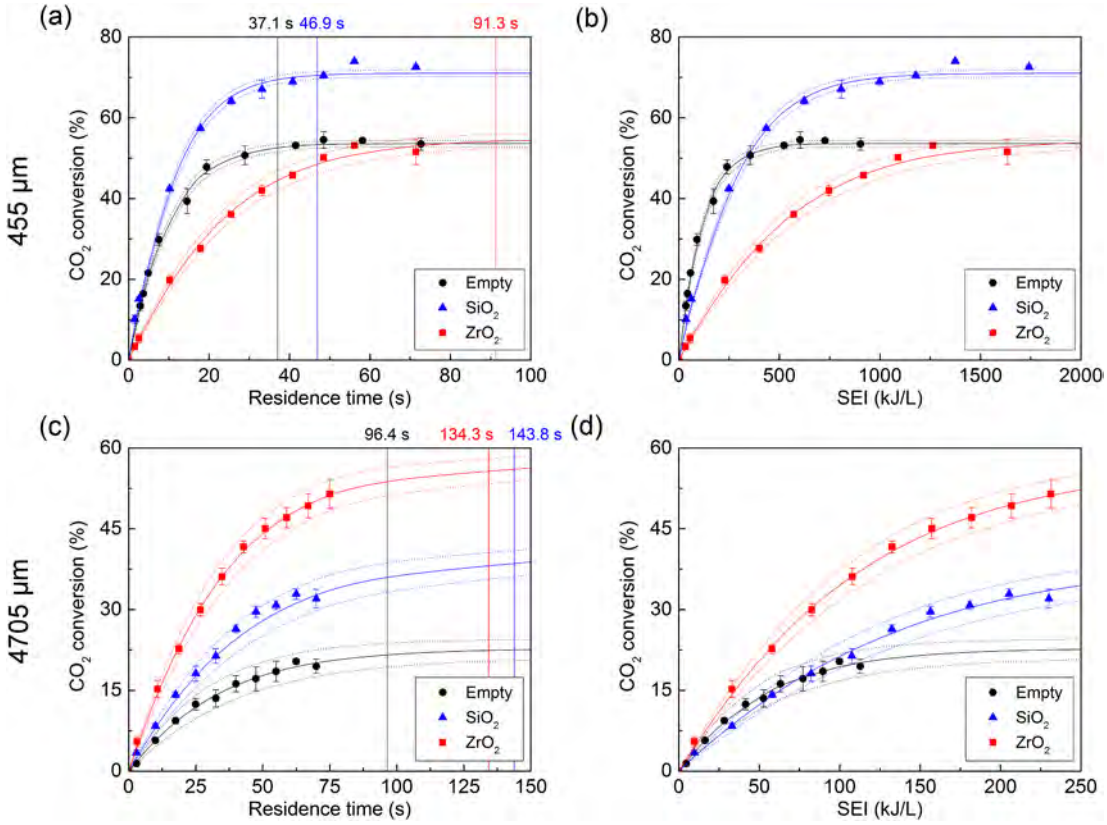

Fig. 4. (a) CO_2 conversion at 30 W, 1 bar, and a gap size of 455 µm, plotted as a function of residence time for an empty reactor, as well as a reactor filled with 100–200 µm spheres of SiO_2 and ZrO_2. (b) CO_2 conversions of (a) rescaled as a function of SEI. (c) CO_2 conversion at 30 W, 1 bar, and a gap size of 4705 µm, plotted as a function of residence time for an empty reactor, as well as a reactor filled with 1600–1800 µm spheres of SiO_2 and ZrO_2. (d) CO_2 conversions of (c) rescaled as a function of SEI. An apparent first-order reversible reaction fit is applied for all graphs (solid lines) with its 95% confidence interval (dotted lines). The time point at which the fit in (a) and (c) reaches 98% of the end conversion of CO_2 dissociation is indicated for each case by the vertical line.

Table 4
Fitted kinetic and equilibrium data for the CO_2 splitting reaction, at an empty reactor as well as a reactor filled with either SiO_2 or ZrO_2 spheres, at 30 W, and 1 bar. The 455 µm gap size is filled with 100–200 µm spheres, while the 4705 µm gap size is filled with 1600–1800 µm spheres. The retrieved data are the equilibrium constant K, calculated from the X_e values, as well as the apparent reaction rate coefficient k, equilibrium conversion X_e, and time to equilibrium conversion t_e.

455 µm gap	Empty[a]	SiO_2	ZrO_2
K	0.28 ± 0.02	1.6 ± 0.1	0.32 ± 0.05
k (s^{-1})	0.120 ± 0.005	0.111 ± 0.004	0.050 ± 0.003
X_e (%)	53.6 ± 0.8	71.1 ± 0.8	55 ± 2
t_e (s)	37.1	46.9	91.3
4705 µm gap	**Empty[b]**	**SiO_2**	**ZrO_2**
K	0.009 ± 0.002	0.07 ± 0.02	0.39 ± 0.08
k (s^{-1})	0.032 ± 0.005	0.027 ± 0.003	0.034 ± 0.002
X_e (%)	23 ± 2	40 ± 2	57 ± 2
t_e (s)	96.4	143.8	134.3

a, b: Denoted as standard reference A and B throughout all measurements.

catch up, and the SiO_2 packing performs better than the empty reactor at around 300 kJ/L because of its higher equilibrium conversion. This shows that one should carefully investigate the kinetics and equilibria, to try to work at optimum conditions for a specific application, especially with packed plasma reactors.

It is interesting to note that studying the effect of packing materials at only one, or a limited number of residence time(s), would not reveal any catalytic activity or whether the packing material enhances either the rate or the equilibrium of the reaction. Our approach allows us to conclude that SiO_2 improves on the empty reactor only because of its equilibrium enhancement and not by kinetics enhancement (slightly overlapping error bars). The empty reactor, on the other hand, is better than ZrO_2 only because of rate inhibition by ZrO_2 and not because of any equilibrium changes.

3.3.2. *Influence of packing material in a 4705 µm discharge gap*

The second set of experiments was performed with a 4705 µm gap size, again with either SiO_2 or ZrO_2 spheres with a size range of 1600–1800 µm, and the results were again compared to the empty 4705 µm reactor from Section 3.2.3. This combination of gap size and sphere sizes was also used in our previous work, as the benchmark, where different trends were found than those observed in Section 3.3.1, with both SiO_2 and ZrO_2 being able to enhance the CO_2 conversion (i.e. 10% and 14%, respectively) as compared to the empty reactor (4%) at a constant residence time of 7.5 s [14]. Interestingly, ZrO_2 showed even better results than SiO_2 in these experiments. Here, we performed similar experiments to the work in [14], but in the whole residence time range, and the results are shown in Fig. 4(c) with the retrieved data in Table 4.

These data confirm the trends observed in [14], with ZrO_2 leading to the highest conversions, followed by SiO_2 and finally the empty reactor. This translates in respective equilibrium conversions of 57, 40, and 23% (see Table 4). In contrast to the smaller gap, the kinetics seem not to be greatly affected by the packing materials in this gap size, showing rate coefficients around 0.031 s^{-1} with overlapping error bars. This suggests that there is no apparent catalytic effect for these packing materials and this particular reaction, as the packing material only changes the equilibrium and not the kinetics. Again, no rate

enhancement is seen due to the reduced discharge gap. Van Laer and Bogaerts [40] indeed showed in their work that the electron density and the CO_2 dissociation rate in a millimetre gap (4.5 mm, hence very similar as used here) are much less affected by the dielectric constant of the packing beads (*ergo* constant rate coefficient), while the electron temperature certainly is (*ergo* change in PCE). It can be noted that the time to reach equilibrium does show some variance despite the similar rate coefficients, due to higher equilibrium and K values. It is clear from the results from both gap sizes that there is an important material-gap-interaction dictating the behaviour of the plasma, i.e. electric field, electron temperature, and electron density, as was also revealed by numerical modelling [40]. However, the origin of the change in material order is not clear at this moment. Since the modelling results were for a helium DBD and no specific material properties could be incorporated, except for the dielectric constant. Moreover, we could not perform detailed plasma diagnostics in this packed bed DBD, and the electric characterization showed no different behaviour, as demonstrated in our previous work [14]. Hence, the underlying reason for the different behaviour will require further investigations.

In contrast to the small gap, rescaling the results as a function of the SEI shows that a ZrO_2-packed DBD reactor will always show the most efficient conversion for a certain CO_2 flow rate, see Fig. 4(d). The empty reactor performs better than the SiO_2-packed reactor at low SEI because of its slightly higher rate coefficient, but the order is switched at around 75 kJ/L, as the equilibrium conversion is higher. Just like we concluded in Section 3.3.1, it is clear that such information could not be obtained from measurements at fixed residence time, namely that the improved results seen at any particular residence time only originate from changes in the equilibrium and not from kinetics enhancement.

3.4. A common underlying connection, or a more complicated story?

Sections 3.2 and 3.3 have shown that both the process parameters (power, pressure and gap size) as well as the packing materials can influence the kinetics and/or equilibrium of the CO_2 dissociation reaction. The exact origin and connection of these effects is, however, less clear. Plotting the equilibrium constant and rate coefficients as a function of the estimated reduced electric field E/N for each condition does give us some clues, see Fig. 5. Note that the reduced electric field is indeed often used as a crucial parameter in plasma-based gas conversion experiments, as it determines the electron temperature, which defines the CO_2 equilibrium conversion and energy efficiency [5,41]. E/N is calculated here according to:

$$\frac{E}{N} = \frac{\frac{U_{RMS}}{d}}{N} \tag{9}$$

With U_{RMS} the effective (or root mean square) voltage, d the gap size, and N the gas density of an ideal gas at the given pressure, i.e. $2.5 \times 10^{25}\,m^{-3}$ at 1 atm. Note that E/N is mostly expressed in Td, with $10^{-21}\,Vm^2$ corresponding to 1 Td.

When changing power, pressure, or gap size, the equilibrium constant and overall rate coefficient appear to move in the same direction, as shown in Fig. 5. For example, an increase of overall rate coefficient coincides with a higher equilibrium constant. This correlation suggests that kinetics and equilibrium cannot be independently tuned (at least for this process and this reactor) purely by changing operating conditions. Introduction of a packing, however, breaks this trend: the overall rate coefficient decreases, compared to the empty reactor, but the equilibrium constant (and equilibrium conversion) goes up. Hence, for this particular setup, we can infer that packing materials bring the plasma to a new regime that allows for a more flexible process optimization.

The question arises how the plasma couples to the gas phase chemistry? As mentioned above, the reduced electric field can be used as a measure for the electron temperature, and as electron impact

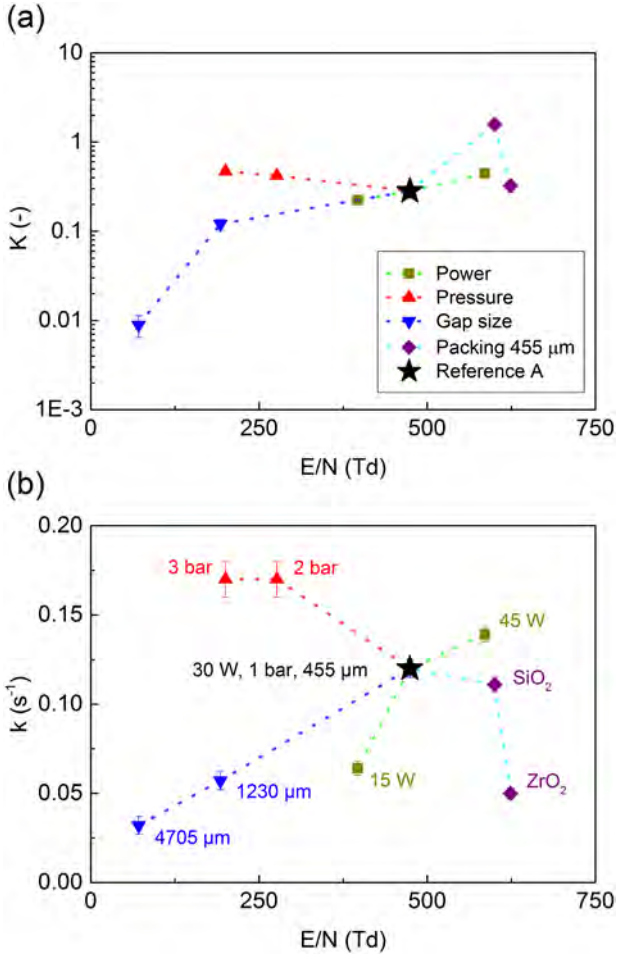

Fig. 5. Combined graph of the (a) equilibrium constants and (b) reaction rate coefficients of Sections 3.2 and 3.3, plotted as a function of the estimated reduced electric field (E/N). All the results are compared against the reference empty reactor A (see tables above). The conditions correlated to the E/N are only annotated in (b) but can be inferred to (a). An additional version with the packed reactor data from 4705 µm can be found in Fig. SI3 in the Supporting Information.

dissociation is the main dissociation mechanism in a DBD reactor [9], the electron temperature can be seen as the main source of energy for CO_2 splitting in a DBD plasma reactor. More energy should therefore translate into more conversion, since it pushes the equilibrium to the right for this endothermic reaction, and this is what we observe at constant pressure and without packing, in conjunction with an increasing reaction rate (see Fig. 5).

However, this trend is not observed when varying the pressure. Hence, there must be some other parameters that dictate the behaviour of the rate coefficient. A first parameter to consider is the electron density. A higher pressure will lead to a lower E/N, and thus lower electron temperature, but also to a higher density of all species, including the electron density. This might thus enhance the CO_2 dissociation rate, and compensate for the lower E/N, and thus lower electron temperature. Moreover, the similarities in the behaviour of the rate coefficient and equilibrium constant for the non-packed reactor suggest that kinetic and equilibrium effects are strongly intertwined, and especially a good understanding of kinetics is required.

Trends for the packed reactors are even harder to discern. First, there is some uncertainty in defining the true exact reduced electric field between the spheres as the total applied voltage is dispersed over all the voids between the spheres. In addition, some possible surface effects might also play a role, such as charging, sorption, local field

enhancement, etc. so the effective voltage is still used here. As mentioned in Section 3.3.1 and shown by Van Laer and Bogaerts [40], using packing materials can greatly change the electron density, due to their dielectric constant, with the actual magnitude of the effect depending on the gap size, influencing the overall rate coefficient. Furthermore, using packing materials increases the surface area in contact with the plasma, possibly causing some surface losses and the same effects as above. Secondly, aside from the electron density, there might be (as of yet unknown) other parameters that can influence the overall rate coefficient of CO_2 conversion, which may be especially hard to determine in a packed reactor. Changing from one packing material to another will of course change multiple other packing properties as well, besides the dielectric constant. These consist of (i) bulk properties of the material, such as size, shape, electric conductivity, thermal capacity, and thermal conductivity, as well as (ii) surface properties, such as crystal phases, roughness, pore size, and functional groups, among others. Their exact effect on the overall rate coefficient, as well as on the equilibrium constant, is very difficult or even impossible to evaluate individually, in addition to the entangled nature of the plasma–material interaction [26,27]. Thirdly, we can consider any catalytic behaviour occurring when using a packing. Our study, as discussed in Section 3.3, reveals no apparent catalytic behaviour for bare SiO_2 and ZrO_2 in the CO_2 dissociation reaction. However, these materials seem to change the plasma properties more than any catalytic rate coefficient enhancement, unless masked so much by the other changes.

The key importance of kinetics and its correlation to the equilibrium can also be found in our simplified kinetics model, see Section 2.3. From the detailed derivation of Eq. (6) in the SI, it follows that both the overall conversion rate coefficient k_y and the equilibrium concentration x_e of any product can be expressed as a function of its global consumption rate coefficient k_1 and its global production rate coefficient k_2. More specifically, the overall rate coefficient k_y is proportional to the sum of k_1 and k_2 ($k_y = k_1 + k_2$ according to Eq. (SI33)), while $x_{e,y} = k_2/(k_1 + k_2)$ (according to Eq. (SI34)) — ignoring any coefficients due to stoichiometry for the sake of clarity.

In thermal catalysis, the activation energy of both consumption and production is lowered equally, and both k_1 and k_2 increase by the same factor. This means that the global conversion rate can increase (still $k_y = k_1 + k_2$), but the thermal equilibrium concentration cannot ($K_T = k_2/k_1$ must remain constant, and hence $x_{e,T}$ cannot change), as is also shown by our model equations. However, many of the results in this work demonstrate that in the non-equilibrium environment of the plasma reactor, also the equilibrium concentration can change. This is the result of k_1 and k_2 changing independently. For example, in our packed reactors we have observed that the overall rate did not increase appreciably (it even decreased in some cases): these results can be attributed to an increased CO_2 decomposition rate, compensated by a decreased CO_2 production rate, keeping the sum of the rates constant. Hence, in contrast to traditional catalytic approaches, where forward and reverse reaction rates are modified in the same fashion, plasma (catalysis) can modify each of these rates independently and thus the overall rate coefficient both positively and negatively; and at the same time changing the position of the equilibrium by an altered correlation as described by Eq. (SI34). Future endeavours in this field could therefore attempt to target specific reactions, allowing to increase both the production rate and equilibrium concentration of a desired product.

In the end, for both thermal (catalytic) processes and plasma (catalytic) processes, net energy is provided to the system. It should therefore be possible to define a clear correlation between plasma power and equilibrium, as well as rate coefficient, as is the case for thermal processes. The reality is, however, more complicated since clearly multiple parameters influence how this power is delivered to a system. Not only input power shifts the equilibrium, but also the gap, pressure, and packing materials. At the same time, the plasma characteristics can also change such as: vibrational versus electronic excitation, magnitude and frequency of discharges, electron temperature and density, etc. Therefore, there is a clear difference between the limited control options of thermal (only temperature and pressure), versus the wide control options in case of plasma.

3.5. Future potential of PCE studies

In this work we investigated the existence of a PCE in a DBD plasma reactor, we verified how it is affected by reactor and packing parameters, and we reviewed the associated kinetics by using an apparent first-order reversible reaction fit equation. In this first proof-of-concept of our method, very valuable information was obtained, even for the simple but paradigmatic CO_2 splitting reaction with non-porous packing materials, i.e. SiO_2 and ZrO_2. Our novel analysis methodology can be a valuable tool in future research, regardless of the specific plasma research area. It is able to yield process parameters that allow for a comparison of different plasma reactor types, set-ups, reactions, and packing materials, which is very useful, especially considering the huge diversity in published plasma-based conversion experiments in which the role of certain reaction configurations and introduced materials is often only visible as a mere positive or negative effect.

Furthermore, specific reactions ask for specific needs and conditions, which, to some extent, can be selected and optimized through our proposed procedure. Also here, the rate coefficient and position of the equilibrium are essential in understanding the overall chemistry allowing some insights to optimize the reaction. Depending on the reaction, it allows to determine the conditions to achieve a certain conversion level, predict the time evolution of the composition, and possibly steer the product distribution in more complicated mixtures. Additionally, the presence, or lack, of a catalytic effect can be investigated: candidate catalysts can be systematically screened (e.g. on composition, available surface area, and doped elements), for their impact on rate or PCE, and their application in plasma-based conversion processes can be readily compared with pure plasma processes, as well as thermal catalysis.

Untangling the highly complex physical chemistry of plasma-catalytic conversion processes, and comparing it with the well-known processes in thermal catalysis, requires a strategic (stepwise) analysis, based on well-defined and preferably easy to obtain fundamental insights, such as those provided by the method suggested in this work. Combination of this approach with more detailed experimental diagnostics and computational modelling, if available, can therefore bring our understanding to the next level, in the quest for new advanced gas conversion technologies.

4. Conclusion

In this paper we have shown that a partial chemical equilibrium does exists in a DBD (micro) plasma reactor, as both the forward (pure CO_2) and back reaction (2/3 CO + 1/3 O_2) converge to a common equilibrium state upon increasing residence time. Furthermore, by performing experiments within an extended range of residence times, and developing an apparent first-order reversible reaction fit equation, we can describe the operational behaviour of the reactor and retrieve essential kinetics and thermodynamics data from the experimental results. This way we could determine equilibrium concentrations and constants, (overall) rate coefficients, and the presence or absence of catalysis of chemical processes in the inherently non-thermal-equilibrium environment of a plasma, that could otherwise not be described.

Analysis of the effect of different process parameters (i.e., power, pressure, and gap size) on the equilibrium and rate coefficient, showed that a higher power shifts the equilibrium in the forward direction and enhances the rate. The pressure showed a different effect, with a drop for the equilibrium conversion and a rise for the rate coefficient, upon increasing pressure. Finally, decreasing the gap size has a general positive effect, drastically enhancing the equilibrium conversion and the rate coefficient.

When inserting a packing (SiO_2 and ZrO_2 spheres), a clear gap/material effect becomes apparent. In the case of the 455 µm gap, the SiO_2-packed reactor showed better conversions than the empty reactor due to a shift of the equilibrium, and not by enhancement of the kinetics. ZrO_2, on the other hand, showed worse results, because of a drop in the rate while maintaining the same equilibrium conversion. In the case of the 4705 µm gap, we observed no significant effect on the rate coefficients for both materials, while the equilibrium conversion was enhanced for both the SiO_2 and ZrO_2 packings. Interestingly, ZrO_2 performed better than SiO_2 in the larger gap indicating important material-gap-interactions on the kinetics. Hence, in general, both packing materials did not positively affect the rate coefficients compared to the empty reactors in both gap sizes, while either increasing or decreasing the equilibrium conversion, and thus enhancing or inhibiting some plasma properties. It is therefore not possible to declare any apparent synergistic effect or plasma-catalytic behaviour from these results for SiO_2 and ZrO_2 in CO_2 dissociation.

Our method therefore reveals an intriguing opportunity to independently tune the equilibrium conversion and rate coefficient, depending on the plasma and process parameters. Within the investigated parameter ranges, equilibrium conversions were obtained between 23 and 71%; to our knowledge, 71% is the highest value reported up to now for a DBD reactor (although accompanied by a low energy efficiency). The reduced electric field E/N was shown to have a prominent underlying effect in determining the equilibrium conversion, as a higher E/N yields a higher electron temperature, which is the main energy source for CO_2 splitting in a DBD plasma, therefore shifting the equilibrium of this endothermic reaction to the right. The rate coefficient, on the other hand, varied between 0.027 s^{-1} and 0.17 s^{-1}, being determined by more underlying effects apart from the reduced electric field.

In conclusion, the proposed definition of an effective global rate coefficient (here for the CO_2 splitting reaction), in combination with the partial chemical equilibrium constant, can be used to characterize the intrinsic properties of a conversion process in a plasma reactor, and directly compare the performance of different conditions and set-ups on a fundamental level. Depending on the desired properties (e.g., high equilibrium conversion vs. high rates), such performance indicators can be used to select or optimize the operating conditions. We therefore advise to implement similar analyses in other plasma-based gas conversion studies, and especially when studying the mechanisms behind plasma catalysis, to obtain a more fundamental insight in the overall reaction kinetics and being able to distinguish plasma effects from true catalytic enhancement.

Acknowledgements

The authors acknowledge financial support from the European Fund for Regional Development through the cross-border collaborative Interreg V program Flanders-the Netherlands (project EnOp), the Fund for Scientific Research (FWO; Grant Number: G.0254.14N), a TOP-BOF project and an IOF-SBO (SynCO2Chem) project from the University of Antwerp. K. M. B. was funded as a PhD fellow (aspirant) of the FWO-Flanders (Fund for Scientific Research-Flanders), Grant 11V8915N.

Appendix A. Supplementary data

Supplementary data to this article can be found online at https://doi.org/10.1016/j.cej.2019.05.008.

References

[1] H.-H. Kim, Nonthermal plasma processing for air-pollution control: a historical review, current issues, and future prospects, Plasma Process. Polym. 1 (2004) 91–110, https://doi.org/10.1002/ppap.200400028.
[2] J. Van Durme, J. Dewulf, C. Leys, H. Van Langenhove, Combining non-thermal plasma with heterogeneous catalysis in waste gas treatment: a review, Appl. Catal., B 78 (2008) 324–333, https://doi.org/10.1016/j.apcatb.2007.09.035.
[3] U. Kogelschatz, B. Eliasson, W. Egli, From ozone generators to flat television screens: history and future potential of dielectric-barrier discharges, Pure Appl. Chem. 71 (1999) 1819–1828, https://doi.org/10.1351/pac199971101819.
[4] U. Kogelschatz, Dielectric-barrier: discharges: their history, discharge physics, and industrial applications, Plasma Chem. Plasma Process. 23 (2003) 1–46.
[5] R. Snoeckx, A. Bogaerts, Plasma technology – a novel solution for CO_2 conversion? Chem. Soc. Rev. 46 (2017) 5805–5863, https://doi.org/10.1039/C6CS00066E.
[6] R. Snoeckx, A. Rabinovich, D. Dobrynin, A. Bogaerts, A. Fridman, Plasma-based liquefaction of methane: the road from hydrogen production to direct methane liquefaction, Plasma Process. Polym. 14 (2017) e1600115, , https://doi.org/10.1002/ppap.201600115.
[7] B.S. Patil, Q. Wang, V. Hessel, J. Lang, Plasma N_2-fixation: 1900–2014, Catal. Today 256 (2015) 49–66, https://doi.org/10.1016/j.cattod.2015.05.005.
[8] U. Kogelschatz, Applications of microplasmas and microreactor technology, Contrib. Plasma Phys. 47 (2007) 80–88, https://doi.org/10.1002/ctpp.200710012.
[9] R. Aerts, W. Somers, A. Bogaerts, Carbon dioxide splitting in a dielectric barrier discharge plasma: a combined experimental and computational study, ChemSusChem 8 (2015) 702–716, https://doi.org/10.1002/cssc.201402818.
[10] I. Michielsen, Y. Uytdenhouwen, J. Pype, B. Michielsen, J. Mertens, F. Reniers, V. Meynen, A. Bogaerts, CO_2 dissociation in a packed bed DBD reactor: first steps towards a better understanding of plasma catalysis, Chem. Eng. J. 326 (2017) 477–488, https://doi.org/10.1016/j.cej.2017.05.177.
[11] X. Duan, Z. Hu, Y. Li, B. Wang, Effect of dielectric packing materials on the decomposition of carbon dioxide using DBD microplasma reactor, AIChE J. 61 (2015) 898–903, https://doi.org/10.1002/aic.
[12] D. Mei, X. Zhu, Y. He, J.D. Yan, X. Tu, Plasma-assisted conversion of CO_2 in a dielectric barrier discharge reactor: understanding the effect of packing materials, Plasma Sources Sci. Technol. 24 (2015) 15011, https://doi.org/10.1088/0963-0252/24/1/015011.
[13] A. Ozkan, A. Bogaerts, F. Reniers, Routes to increase the conversion and the energy efficiency in the splitting of CO_2 by a dielectric barrier discharge, J. Phys. D. Appl. Phys. 50 (2017) 084004, , https://doi.org/10.1088/1361-6463/aa562c.
[14] Y. Uytdenhouwen, S. Van Alphen, I. Michielsen, V. Meynen, P. Cool, A. Bogaerts, A packed-bed DBD micro plasma reactor for CO_2 dissociation: does size matter? Chem. Eng. J. 348 (2018) 557–568, https://doi.org/10.1016/j.cej.2018.04.210.
[15] X. Tu, J.C. Whitehead, Plasma-catalytic dry reforming of methane in an atmospheric dielectric barrier discharge: understanding the synergistic effect at low temperature, Appl. Catal., B 125 (2012) 439–448, https://doi.org/10.1016/j.apcatb.2012.06.006.
[16] D. Mei, B. Ashford, Y.L. He, X. Tu, Plasma-catalytic reforming of biogas over supported Ni catalysts in a dielectric barrier discharge reactor: effect of catalyst supports, Plasma Process. Polym. 14 (2017), https://doi.org/10.1002/ppap.201600076.
[17] R. Snoeckx, Y.X. Zeng, X. Tu, A. Bogaerts, Plasma-based dry reforming: improving the conversion and energy efficiency in a dielectric barrier discharge, RSC Adv. 5 (2015) 29799–29808, https://doi.org/10.1039/C5RA01100K.
[18] N. Pinhão, A. Moura, J.B. Branco, J. Neves, Influence of gas expansion on process parameters in non-thermal plasma plug-flow reactors: a study applied to dry reforming of methane, Int. J. Hydrogen Energy 41 (2016) 9245–9255, https://doi.org/10.1016/j.ijhydene.2016.04.148.
[19] S. Kameshima, K. Tamura, Y. Ishibashi, T. Nozaki, Pulsed dry methane reforming in plasma-enhanced catalytic reaction, Catal. Today 256 (2015) 67–75, https://doi.org/10.1016/j.cattod.2015.05.011.
[20] S. Vepřek, Statistical model of chemical reactions in nonisothermal low pressure plasma, J. Chem. Phys. 57 (1972) 952–959, https://doi.org/10.1063/1.1678345.
[21] S. Vepřek, W. Peier, Chemical equilibrium in nonisothermal low pressure plasma, Chem. Phys. 2 (1973) 478–484, https://doi.org/10.1016/0301-0104(73)80024-2.
[22] J.J. Wagner, S. Vepřek, Kinetic study of the heterogeneous Si/H system under low-pressure plasma conditions by means of mass spectrometry, Plasma Chem. Plasma Process. 2 (1982) 95–107, https://doi.org/10.1007/BF00566860.
[23] L. Wang, Y. Yi, C. Wu, H. Guo, X. Tu, One-step reforming of CO_2 and CH_4 into high-value liquid chemicals and fuels at room temperature by plasma-driven catalysis, Angew. Chem. Int. Ed. 56 (2017) 13679–13683, https://doi.org/10.1002/anie.201707131.
[24] A.M. Vandenbroucke, R. Morent, N. De Geyter, C. Leys, Non-thermal plasmas for non-catalytic and catalytic VOC abatement, J. Hazard. Mater. 195 (2011) 30–54, https://doi.org/10.1016/j.jhazmat.2011.08.060.
[25] J.C. Whitehead, Plasma – catalysis: the known knowns, the known unknowns and

the unknown unknowns, J. Phys. D. Appl. Phys. 49 (2016) 243001, , https://doi.org/10.1088/0022-3727/49/24/243001.
[26] E.C. Neyts, K. Ostrikov, M.K. Sunkara, A. Bogaerts, Plasma catalysis: synergistic effects at the nanoscale, Chem. Rev. 115 (2015) 13408–13446, https://doi.org/10.1021/acs.chemrev.5b00362.
[27] E.C. Neyts, A. Bogaerts, Understanding plasma catalysis through modelling and simulation—a review, J. Phys. D. Appl. Phys. 47 (2014) 224010, , https://doi.org/10.1088/0022-3727/47/22/224010.
[28] Y.R. Zhang, K. Van Laer, E.C. Neyts, A. Bogaerts, Can plasma be formed in catalyst pores? A modeling investigation, Appl. Catal., B 185 (2016) 56–67, https://doi.org/10.1016/j.apcatb.2015.12.009.
[29] Q.-Z. Zhang, A. Bogaerts, Propagation of a plasma streamer in catalyst pores, Plasma Sources Sci. Technol. 27 (2018) 035009, , https://doi.org/10.1088/1361-6595/aab47a.
[30] Q.-Z. Zhang, W.-Z. Wang, A. Bogaerts, Importance of surface charging during plasma streamer propagation in catalyst pores, Plasma Sources Sci. Technol. 27 (2018) 065009, , https://doi.org/10.1088/1361-6595/aaca6d.
[31] R. Snoeckx, S. Heijkers, K. Van Wesenbeeck, S. Lenaerts, A. Bogaerts, CO_2 conversion in a dielectric barrier discharge plasma: N_2 in the mix as a helping hand or problematic impurity? Energy Environ. Sci. Energy Environ. Sci. 9 (2016) 999–1011, https://doi.org/10.1039/c5ee03304g.
[32] R. Aerts, T. Martens, A. Bogaerts, Influence of vibrational states on CO_2 splitting by dielectric barrier discharges, J. Phys. Chem. C 116 (2012) 23257–23273, https://doi.org/10.1021/jp307525t.
[33] T. Kozák, A. Bogaerts, Splitting of CO_2 by vibrational excitation in non-equilibrium plasmas: a reaction kinetics model, Plasma Sources Sci. Technol. 23 (2014) 045004, , https://doi.org/10.1088/0963-0252/23/4/045004.
[34] A. Berthelot, A. Bogaerts, Modeling of CO_2 plasma: effect of uncertainties in the plasma chemistry, Plasma Sources Sci. Technol. 26 (2017) 115002, , https://doi.org/10.1088/1361-6595/aa8ffb.
[35] S. Kolev, A. Bogaerts, A 2D model for a gliding arc discharge, Plasma Sources Sci. Technol. 24 (2014) 015025, , https://doi.org/10.1088/0963-0252/24/1/015025.
[36] A. Berthelot, A. Bogaerts, Modeling of CO2 splitting in a microwave plasma: how to improve the conversion and energy efficiency, J. Phys. Chem. C 121 (2017) 8236–8251, https://doi.org/10.1021/acs.jpcc.6b12840.
[37] F. Paschen, Ueber die zum Funkenübergang in Luft, Wasserstoff und Kohlensäure bei verschiedenen Drucken erforderliche Potentialdifferenz, Ann. Phys. 273 (1889) 69–96, https://doi.org/10.1002/andp.18892730505.
[38] K. Van Laer, A. Bogaerts, How bead size and dielectric constant affect the plasma behaviour in a packed bed plasma reactor: a modelling study, Plasma Sources Sci. Technol. 26 (2017) 085007, , https://doi.org/10.1088/1361-6595/aa7c59.
[39] W. Wang, H.H. Kim, K. Van Laer, A. Bogaerts, Streamer propagation in a packed bed plasma reactor for plasma catalysis applications, Chem. Eng. J. 334 (2018) 2467–2479, https://doi.org/10.1016/j.cej.2017.11.139.
[40] K. Van Laer, A. Bogaerts, Influence of gap size and dielectric constant of the packing material on the plasma behaviour in a packed bed DBD reactor: a fluid modelling study, Plasma Process. Polym. 14 (2017) 1600129, https://doi.org/10.1002/ppap.201600129.
[41] A. Bogaerts, T. Kozák, K. van Laer, R. Snoeckx, Plasma-based conversion of CO2: current status and future challenges, Faraday Discuss. 183 (2015) 217–232, https://doi.org/10.1039/C5FD00053J.